Anodizing of Self-Passivating WxTi1–x Precursors for WxTi1–xOn Oxide Alloys with Tailored Stability

Siol, Sebastian ; Beall, Casey ; Ott, Noémie ; Döbeli, Max ; González-Castaño, Miriam ; Wick-Joliat, René ; Tilley, S David ; Jeurgens, Lars P H ; Schmutz, Patrik ; Cancellieri, Claudia

Abstract: TiO2 and WO3 are two of the most important, industrially relevant earth-abundant oxides. Although both materials show complementary functionality and are promising candidates for similar types of applications such as catalysis, sensor technology, and energy conversion, their chemical stability in reactive environments differs remarkably. In this study, anodic barrier oxides are grown on solid-solution WxTi1–x alloy precursors covering a wide compositional range (0 x 1) with the goal of creating functional oxides with tailored stability. A strong Ti-cation enrichment in the surface region of the grown WxTi1–xOn layer is observed, which can be controlled by both the anodizing conditions and precursor composition. For Ti concentrations above 50 at. %, a continuous nanometer-thick TiO2 protective coating is achieved on top of a homogeneous WxTi1–xOn film as evidenced by X-ray photoelectron spectroscopy and transmission electron microscopy analyses. A comprehensive electrochemical assessment demonstrates a very stable passivation of the surface in both acidic and alkaline environments. This increase in chemical stability correlates directly with the presence of this protective TiO2 film. The results of this work provide insights into the oxidation behavior of W1–xTix alloys, but more importantly demonstrate how controlled oxidation of self-passivating alloys can lead to oxide alloys with thin, protective surface layers that otherwise would require more sophisticated deposition methods.

DOI: https://doi.org/10.1021/acsami.8b19170

Anodizing of self-passivating W_xTi_{1-x} precursors for $W_xTi_{1-x}O_n$ oxide alloys with tailored stability

Sebastian Siol[a,*], Casey Beall[a,b], Noémie Ott[a], Max Döbeli[c], Miriam González-Castaño[a], René Wick-Joliat[b], S. David Tilley[b], Lars P.H. Jeurgens[a], Patrik Schmutz[a], Claudia Cancellieri[a]

[a]Empa - Swiss Federal Laboratories for Materials Science and Technology, Überlandstrasse 129, 8600 Dübendorf, Switzerland

[b]University of Zurich, Department of Chemistry, Winterthurerstrasse 190, 8057 Zurich, Switzerland

[c]ETH Zurich, Ion Beam Physics, Otto-Stern-Weg 5, 8093 Zurich, Switzerland

*E-Mail: Sebastian.Siol@empa.ch

Abstract:

TiO_2 and WO_3 are two of the most important, industrially relevant earth-abundant oxides. While both materials show complementary functionality, and are promising candidates for similar types of applications such as catalysis, sensor technology and energy conversion, their chemical stability in reactive environments differs remarkably. In this study, anodic barrier oxides are grown on solid solution W_xTi_{1-x} alloy precursors covering a wide compositional range ($0 \leq x \leq 1$) with the goal of creating functional oxides with tailored stability. A strong Ti-cation enrichment in the surface region of the grown $W_xTi_{1-x}O_n$ layer is observed, which can be controlled by both the anodizing conditions and precursor composition. For Ti-concentrations above 50 at.%, a continuous nm-thick TiO_2 protective coating is achieved on top of a homogeneous $W_xTi_{1-x}O_n$ film as evidenced by X-Ray photoelectron spectroscopy and transmission electron microscopy analyses. A comprehensive electrochemical assessment demonstrates a very stable passivation of the surface in both acidic and alkaline environments. This increase in chemical stability correlates directly with the presence of this protective TiO_2 film. The results of this work provide insights into the oxidation behavior of $W_{1-x}Ti_x$ alloys, but more importantly demonstrate how controlled oxidation of self-passivating alloys can lead to oxide alloys with thin, protective surface layers that otherwise would require more sophisticated deposition methods.

Keywords:

Oxide alloy, Heterostructure, Barrier anodization, Surface passivation, Tungsten, Titanium

1. Introduction

Technology development for sustainability and renewable energy applications calls for environmentally friendly materials with tailored functionality. Fueled by the stability debate around perovskite solar cells, the need for long term durability in emerging technologies has moved closer to the center of attention in recent years.[1] Besides the obvious performance indicators like photovoltaic conversion efficiency in the case of thin film photovoltaics or the electrochromic glazing efficiency in the case of electrochromic devices, tailoring long term durability in reactive environments is paramount. TiO_2 and WO_3 are two of the most important earth-abundant materials for electronic and energy applications.[2,3] Particularly for smart windows, WO_3 is one of best performing materials to date.[3] TiO_2 and WO_3 show similar functional properties, but at the same time vastly different stability in reactive environments. The range of applications for WO_3 is limited by its low stability in corrosive media.[4–6] TiO_2 on the other hand is stable in most aggressive environments and routinely used as a protective over-layer in energy conversion applications to prevent corrosion from the underlying devices.[7–9] It is this difference in durability, which make $W_xTi_{1-x}O_n$ oxide alloys particularly interesting as a model system for tailoring stability.

Alloying is a commonly employed strategy to tailor materials properties, often with the goal to combine desirable properties exhibited by the alloying-endmember materials. While isoelectronic alloying within the same crystal structure often results in gradual changes of functional properties, alloying of structurally mismatched materials often results in structural transitions, which in turn can lead to discontinuous changes in properties or even new functionalities that none of the endmember materials possess.[10] Such structural changes have previously been reported in heterostructural alloys of WO_3 with TiO_2 alongside promising improvements of the electrochromic glazing efficiency.[11,12] In these works reactive sputtering was used to synthesize the alloys. While non-equilibrium synthesis such as magnetron sputtering or pulsed laser deposition is useful to achieve enhanced solubility through kinetic stabilization at moderate deposition temperatures,[13,14] in many instances oxidation of metallic precursors can offer promising complementary synthesis routes. In contrast to high energy physical vapor deposition processes, the near-equilibrium oxidation of metallic alloy precursors often results in phase segregation, even at relatively small alloying concentrations. While this can be regarded detrimental for some applications, it also offers unique opportunities for controlling the microstructure of the oxide.

Preferential oxidation and self-passivation are phenomena observed in many alloys,[15–18] the best known and most industrially relevant being stainless steel, where chromium oxide is

formed on the surface in corrosive environments inhibiting further dissolution. These mechanisms are commonly utilized to create self-passivating and corrosion resistant metal alloys, e.g. W alloys have been investigated as potential first wall armor for future fusion reactions.[19,20] Preferential oxidation and related decomposition processes can however also be utilized to create multi-layer oxide systems which feature thin and uniform protective surface layers. The ability to form very thin and uniform passivation layers is of potential interest for a number of applications. Particularly, in photo-electrochemical water splitting applications, thin inert oxide layers are routinely used to stabilize the anode material against corrosion[8,21]. As of now, these types of thin, protective surface oxides require expensive deposition techniques like atomic layer deposition[8] and are often prone to structural defects like pinholes or cracks.

With this in mind, we are exploring the intrinsic oxidation and self-passivation behavior of $W_{1-x}Ti_x$ alloy precursors using potentiostatic anodizing. The anodic oxidation of both W and Ti has been extensively discussed in literature, especially in the fields of energy conversion and catalysis.[22–26] While the anodic oxide growth on metal alloys is routinely employed for a variety of precursor chemistries and applications,[27–29] anodizing of $W_{1-x}Ti_x$ is less commonly reported.[30,31] These previous works on the anodic oxidation of $W_{1-x}Ti_x$ alloys focus on the tuning of the oxide morphology and microstructure with the goal to grow nano-porous oxides. In contrast to these studies, we are using barrier anodizing, with the aim to create thin, continuous barrier oxide layers with excellent lateral homogeneity, avoiding pinholes and large scale defects. In a systematic investigation, it is shown how the composition of the precursor and the anodizing conditions influence the properties of the resulting mixed oxide. Depending on the precursor alloy composition, a strong Ti- surface enrichment is observed in the anodic oxide resulting in improved chemical stability in aggressive environments as evidenced by a comprehensive electrochemical impedance spectroscopy (EIS) and potentiodynamic polarization assessment. For Ti-rich precursors an oxide bi-layer is formed consisting of a thin, but continuous TiO_2 surface layer and a homogeneous oxide alloy underneath, providing excellent surface passivation, while still allowing the tuning of functional properties as a function of precursor composition.

The results of this work elucidate the oxidation behavior and self-passivation of the $W_{1-x}Ti_x$ alloy system upon anodizing, but more importantly provide a general design strategy to form functional multilayer oxide systems with tailored properties and chemical stability without the need for secondary coating technologies like atomic layer deposition that can be applied to many other materials systems.

2. Methods

2.1 Synthesis

Metallic thin film precursors were deposited on Si wafers with thin TiN diffusion barriers using DC magnetron sputtering in an AJA 1500-F deposition chamber. The films were sputtered from metallic 2" W and Ti targets (99.95% purity) in pure Ar atmosphere at a process pressure of 5×10^{-3} mbar and a substrate temperature of approximately 350 °C. Single composition samples were deposited using substrate rotation to achieve homogeneous composition and thickness. A wide range of chemical compositions was achieved by adjusting the W and Ti sputter rates by changing the sputter powers in a range from 20 W to 200 W for Ti and 10 W to 80 W for W, respectively. The film thicknesses of the precursors are on the order of 200 nm.

The potentiostatic anodizing of the metal films was carried out in a two electrodes electrochemical cell setup with an exposed area of 1 cm^2 delimited by a silicone O-ring. Citric acid (1 M, adjusted to a pH 5.8) was chosen as electrolyte, since previous work showed that dense barrier oxide containing very low amounts of impurity contamination from the electrolyte can be obtained.[32] The potential was applied between the metallic precursor exposed surface and a Pt counter electrode. The potential was ramped at 6 V/s to the final voltage and subsequently held for 50 s and 100 s for samples anodized at 90 V and 30 V, respectively.

2.2 Characterization

The structures of the precursor alloys as well as oxide films were studied via XRD in a Bruker D8 diffractometer in Bragg Brentano geometry using Cu Kα radiation and a Ni-filter. X-ray photoelectron spectroscopy (XPS) was conducted using a Physical Electronics (PHI) Quantum 2000 X-ray photoelectron spectrometer featuring monochromatic Al Kα radiation, generated from an electron beam operated at 15 kV and 32.3 W. The energy scale of the instrument was calibrated using Au and Cu reference samples. The analysis was conducted at 1×10^{-6} Pa, with an electron take off angle of 45° and pass energies of between 23.50 and 46.95 eV. Surface elemental concentrations were determined in atomic percent using the measured photoelectron peak areas after Shirley background subtraction and the built-in sensitivity factors for calculation. RBS was collected on select samples using a 2 MeV He beam. RUMP simulations were used to determine the films composition. The stoichiometry of the films were normalized using W, Ti = 1 for pure W and Ti precursors and W+Ti = 1 for alloyed precursors. The microstructure and chemical composition of the layer were characterized using

conventional and scanning transmission electron microscopy (S/TEM) combined with energy-dispersive X-ray spectroscopy (EDXS). The TEM sample lamellas were prepared using a focused ion beam (FIB) (FEI Helios Nanolab 450s). A thin Pt layer was deposited via E-beam evaporation prior to the lamella preparation to protect the specimen's surface during FIB preparation. Imaging was performed using a JEOL 2200FS microscope, operated at 200 kV.

For the electrochemical assessment of the reactivity and chemical stability, PVD thin film samples were additionally anodized in an electrochemical cell with a smaller effective area of 0.40 cm^2. Potentiostatic anodizing was carried out at 30 V (5 s ramp from 0-30 V, 100 s holding time at the final potential) in citric acid (pH=5.8). Directly after anodizing, citric acid was exchanged for 1 M NaOH (pH ~13.5) or 1 M H_2SO_4 (pH ~0) for chemical stability characterization in alkaline or acidic conditions, respectively. The further electrochemical characterization is performed in a three electrode cell configuration with an Ag/AgCl reference electrode placed in a Luggin capillary and a platinum counter electrode. First, EIS measurements were repeated every two hours during six hours for frequencies ranging from 10^5 Hz to 2 mHz with an applied voltage amplitude of 10 mV. Potentiodynamic polarization was subsequently performed in 1 M HCl (pH ~0) for samples previously characterized in acidic conditions and 1 M NaOH+1 M NaCl (pH ~13.5) for samples previously characterized in alkaline conditions. The different electrolytes were chosen to expose the sample to increasingly corrosive environments and provoke oxide breakdown at high polarization potentials. The potential was scanned over a wide range from open circuit potential (OCP) to 6 $V_{Ag/AgCl}$ with a scan rate of 1 mV/s. Both EIS and potentiodynamic polarization measurements were performed using a Metrohm Autolab (PGSTAT30 or PGSTAT204) potentiostat. A standard Ag/AgCl reference electrode (Metrohm, 3 M KCl) was used as reference electrode and a Pt ring electrode was used as counter electrode. The potentials are therefore expressed versus Ag/AgCl reference electrode (207 mV_{SHE}).

3. Results and discussion

3.1 Characterization of the $W_{1-x}Ti_x$ alloy precursors

Prior to the anodizing studies, the phase constitution of the sputtered thin film $W_{1-x}Ti_x$ alloys was characterized as a function of alloying element concentration x. **Figure 1** shows X-ray diffraction (XRD) patterns of alloy films for different $W_{1-x}Ti_x$ compositions x deposited on fused silica substrates with TiN diffusion barriers. From Figure 1a, it is apparent that with the

exception of pure Ti (hexagonal closed pack – HCP) all films crystallize in the body centered cubic (BCC) structure. The positions of the (110) and (211) peaks shift as expected with increasing alloying concentration with no visible impurity peaks which would indicate decomposition of the alloy (see **Figure 1b**). A small deviation from the ideal d-spacing evolution according to Vegard's law is observed.[33] This is likely due to stress in the W-rich specimen, as stress measurements on pure W-films revealed a large compressive stress of up to -4 GPa (**Figure S1**). Considering the phase diagram of the Ti-W system, the data suggests formation of a metastable solid solution for most alloying concentrations.[34] These results were confirmed using (S)TEM as well as EDS measurements on a precursor with a nominal composition of $W_{0.3}Ti_{0.7}$ (see **Figure S2**).

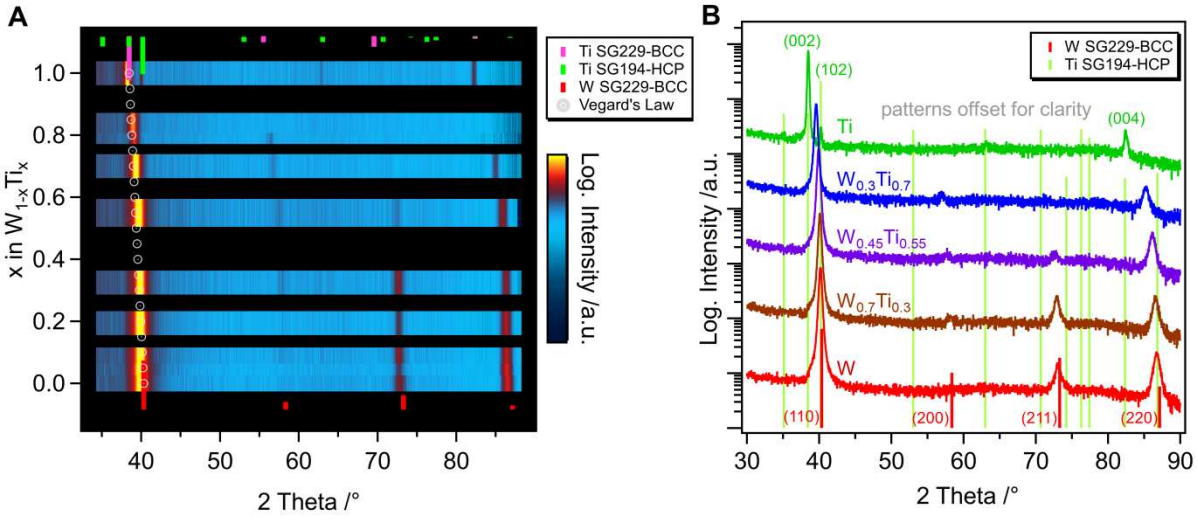

Figure 1: XRD investigation of $W_{1-x}Ti_x$ alloy precursors: a) XRD intensity as a function of alloying concentration *x*. b) 2D plot of individual XRD patterns for W, Ti and $W_{1-x}Ti_x$ alloys at different alloying concentration.

3.2 Anodizing of $W_{1-x}Ti_x$ alloys

In the present study, potentiostatic anodizing was performed to enable control over the energetic environment and the growth rate of the oxide film. A wide variety of different electrolytes was investigated in terms of anodizing behavior and oxide growth rate to achieve equally efficient barrier-anodizing of the two different metals (i.e. Ti and W). One electrolyte that showed qualitatively similar anodizing behavior and comparable oxide growth rates for both W and Ti is 0.1 M citric acid adjusted at a pH of 5.8. Using this electrolyte, current decay transient profiles typical for anodic barrier layer growth are observed for each alloy composition studied (as well as for pure Ti and W) for applied anodizing potentials in the range of 30 to 120 V

(**Figure 2a**). The formation and growth of a barrier oxide layer during the high voltage anodizing process is realized by the electric field stimulated ionic migration of reactants (i.e. cations, anions and their vacancies) through the developing oxide layer under influence of the externally applied voltage. As reflected in Fig. 2, the initial current is proportional to the ramping anodizing voltage, which is typical for the very fast formation of an oxide on the alloy surface at the onset of the anodizing process. However, as soon as the final anodizing voltage is reached, the electric field across the thickening oxide decreases approximately linearly with increasing oxide-layer thickness layer, resulting in an exponential decay of the anodizing current (**Figure 2a**): i.e. a limiting oxide layer thickness is reached. A residual current is observed, which can be related to either a redistribution of ionic and defect species under the influence of the maintained electrical field,[35] or electrolysis processes. These contributions typically vary for different oxides, depending on resistivity, defect chemistry and catalytic performance. **Figure 2b** shows the limiting oxide film thickness obtained from ellipsometry measurements for W and Ti anodized at different voltages. For both Ti and W, similar growth rates of 1.81 nm/V for WO_3 and 1.63 nm/V TiO_2 were observed. The oxide film thickness for an anodized $W_{0.3}Ti_{0.7}$ alloy as determined by TEM analysis, is in good agreement with these growth rates.

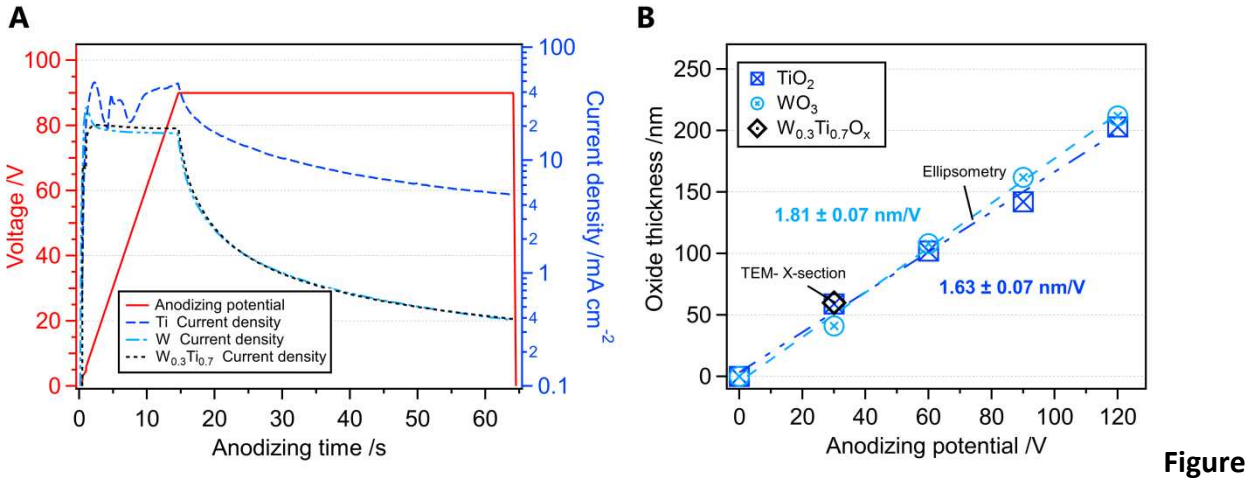

Figure 2: Anodizing behavior of W- and Ti-films: a) Anodizing current-time curves at 90 V anodizing voltage for W, Ti and $W_{0.3}Ti_{0.7}$: barrier oxide growth is observed. b) Ellipsometry measurements show a linear correlation between the oxide film thickness and the applied anodizing voltage. The $W_{0.3}Ti_{0.7}$ alloy oxide thickness from TEM measurements is added for comparison.

XRD analysis of the anodized oxide layers cannot detect any crystalline reflections originating from the oxide layer (i.e. only from the parent alloy substrate) (**Figure S3**). Atomic force microscopy measurements were conducted on the anodized $W_{0.3}Ti_{0.7}$ alloy showing a very smooth surface with a root mean square surface roughness well below 1 nm (**Figure S4**). The

composition of the oxide layers was characterized using Rutherford backscattering spectroscopy (RBS). For anodizing of pure W and Ti, cation to anion ratios close to the respective bulk stoichiometric ratios of 3 for WO_3 and 2 for TiO_2 were measured, respectively (see **Figure S5**). Some excess oxygen compared to stoichiometric WO_3 and TiO_2 found in the oxide films can be explained by inclusion of impurities (e.g. water) into the anodic oxides. XPS analysis of the TiO_2 and WO_3 layers consistently shows Ti 2p and W 4f spectra predominantly composed of Ti^{4+} and W^{6+}, respectively (**Figure S6**).

3.3 Surface composition and self-passivation behavior

The surface chemical composition of the of the $W_{1-x}Ti_x$ alloys was measured by XPS before and after anodizing. The XPS compositional analysis shows a strong deviation of the Ti to W cation-ratio before and after anodizing, revealing a high degree of Ti-enrichment at the oxide surface. Strikingly, this Ti surface enrichment not only depends on the alloy precursor composition, but also on the applied anodizing voltage. **Figure 3** shows the dependence of the Ti-enrichment on both anodizing voltage and precursor composition.

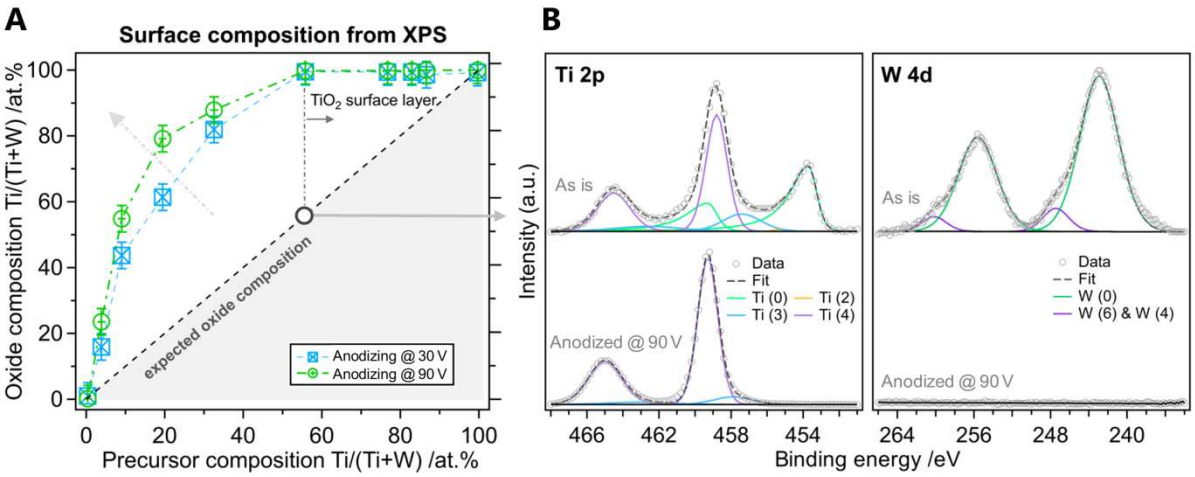

Figure 3: X-ray photoelectron studies on anodized $W_{1-x}Ti_x$ alloys: A) A surface enrichment of Ti at the oxide surface is measured, which strongly depends on the composition and applied anodizing voltage. For Ti ratios over 50% a dense TiO_2 surface layer is formed. The oxide surface composition is displayed on the Y-axis, the precursor surface composition is displayed on the X-axis. B) Spectra of the Ti 2p and W 4d core level emissions measured on $W_{0.45}Ti_{0.55}$ alloys before and after anodizing.

Depending on the precursor alloy composition, higher anodizing voltages result in higher degrees of Ti surface enrichment. If the $W_{1-x}Ti_x$ precursor exceeds a Ti-concentration of approximately x=0.5, a continuous TiO_2 surface layer is formed, which completely attenuates

the underlying W signal as evidenced by XPS measurements of the Ti 2p and W 4d regions (see **Figure 3 B**). In addition, fitting of the Ti 2p core level spectra indicates that mostly Ti^{4+} is present at the oxide surface, while the core level binding energies being in good agreement with literature values for TiO_2. This observation is confirmed by RBS analysis on Ti-rich samples anodized at 90 V (**Figure S5**), which not only show the presence of a TiO_2 surface layer, but also indicate a correlation of the TiO_2 thickness d_{TiO2} with the alloy precursor composition ($d_{TiO2\text{-}30V} \approx 10$ nm, $d_{TiO2\text{-}90V} \approx 20$ nm, see **Figure S5**). Notably, an increase of the holding-time during the anodizing process does not lead to a further increase of the Ti-enrichment at the oxide surface (see **Figure S5** and **Figure S7**). To further investigate the nature of this surface passivation process and the microstructure of the anodic oxide, (S)TEM investigations were carried out on an anodic oxide formed at 30 V on a Ti-rich alloy precursor with a bulk composition of $W_{0.3}Ti_{0.7}$. **Figure 4** shows the results of this analysis. (S)TEM micrographs reveal a bi-layered structure of the oxide layer: a thin TiO_2 surface film of approximately 10 nm thickness (blue region) with a 55 nm-thick mixed oxide layer $W_{1-x}Ti_xO_n$ underneath (green region). Both oxide layers, as well as the parent alloy substrate, show negligibly small (if any) compositional fluctuations in the dark field STEM micrographs (Figure 4C).

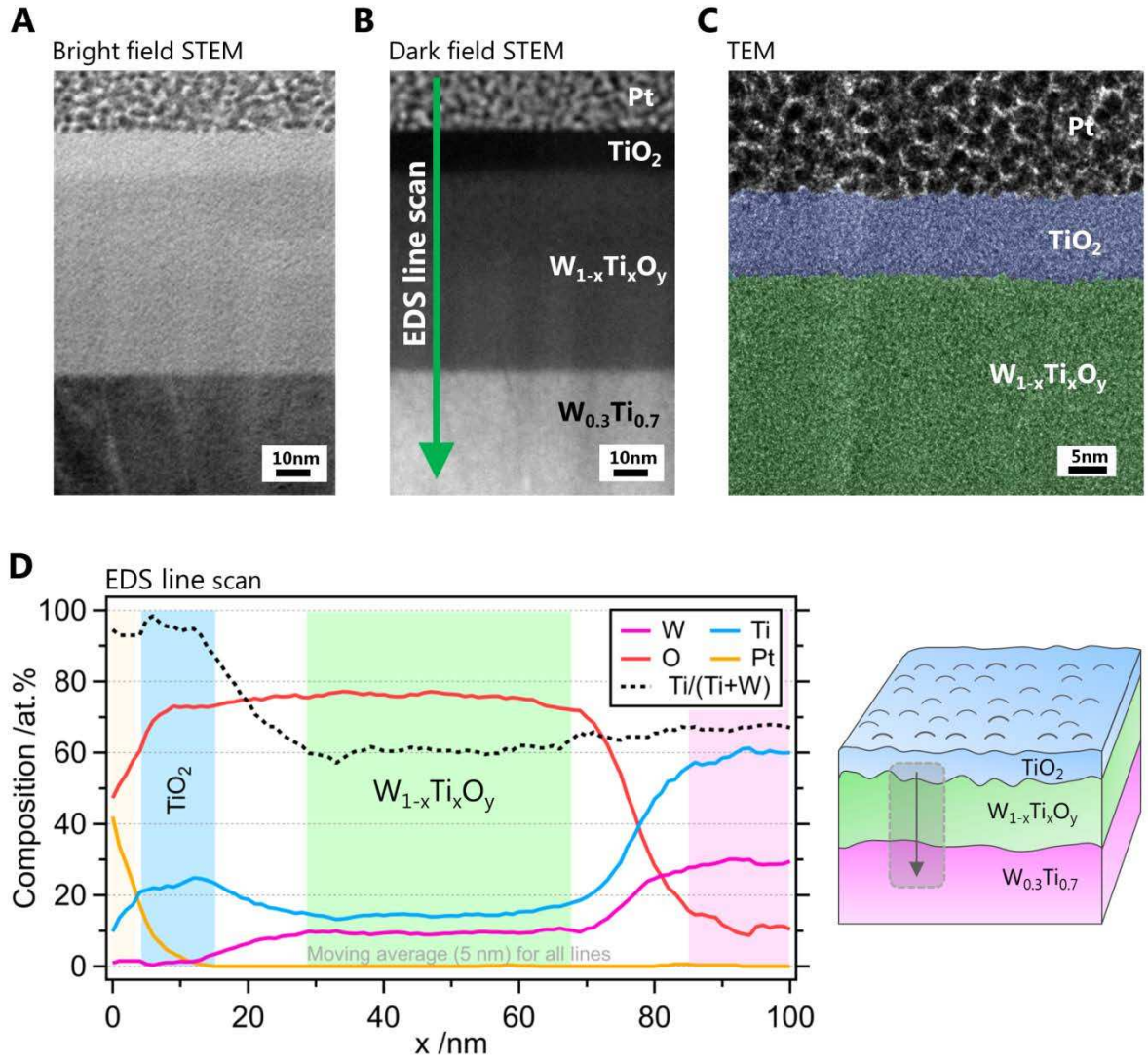

Figure 4: (S)TEM investigation of an anodized $W_{0.3}Ti_{0.7}$ alloy (citric acid, 30V): A,B) Bright field and dark field STEM imaging show four distinct regions: protective Pt coating from FIB sample preparation, TiO_2 surface layer, homogenous mixed oxide region and the parent alloy substrate. C) TEM image of the mixed oxide film and TiO_2 surface layer. Regions are colored for clarity. D) The EDS linescan confirms the presence of a TiO_2 surface layer. The mixed oxide region shows a constant Ti/W ratio close to the precursor composition.

The different compositional regions in the bi-layered oxide were analyzed in more detail by energy dispersive X-ray spectroscopy (EDS) (**Figure 4D**). The TiO_2 surface layer appears stoichiometric with negligible W content. The average composition of the ternary oxide region underneath is approximately $W_{0.4}Ti_{0.6}O_{2.4}$. The metal precursor shows a slightly higher Ti content, which is in good agreement with the average bulk-composition, as determined by RBS. Residual oxygen in the precursor region can be explained by surface oxidation of the TEM

lamella after FIB preparation. Additional XPS depth profiles were performed on the same sample (**Figure S8**), which qualitatively confirm these results. Due to the predominantly amorphous nature of this ternary oxide phase, crystallographic phase identification by TEM (or XRD) is not possible. However, the nominal composition is very close to the ternary oxide phase $Ti_3(WO_6)_2$, which has been predicted at low energy by first principles calculations (40 meV/atom above the convex hull).[36] No nano-sized clusters with a deviating composition (which could indicate decomposition of the oxide alloy into its endmember structures, WO_3 and TiO_2) were detected. In summary, the (S)TEM analysis confirms the formation of a very thin, but dense surface layer of amorphous TiO_2, which is formed on top of a homogenous amorphous ternary oxide phase with a nominal composition of approximately $Ti_3(WO_6)_2$.

3.4 Chemical stability in reactive environments

To assess the chemical stability of the anodic oxides in extreme pH and aggressive electrolytes, a comprehensive electrochemical characterization was carried out. The goal of the study was to expose the samples to increasingly aggressive environments until a breakdown and/or dissolution of the oxide is observed. The measurement procedure and sequence is outlined in **Figure S9**.

In a first step, electrochemical impedance spectroscopy at OCP was conducted in either 1 M H_2SO_4 for acidic conditions or 1 M NaOH for alkaline conditions (see Supporting Information).

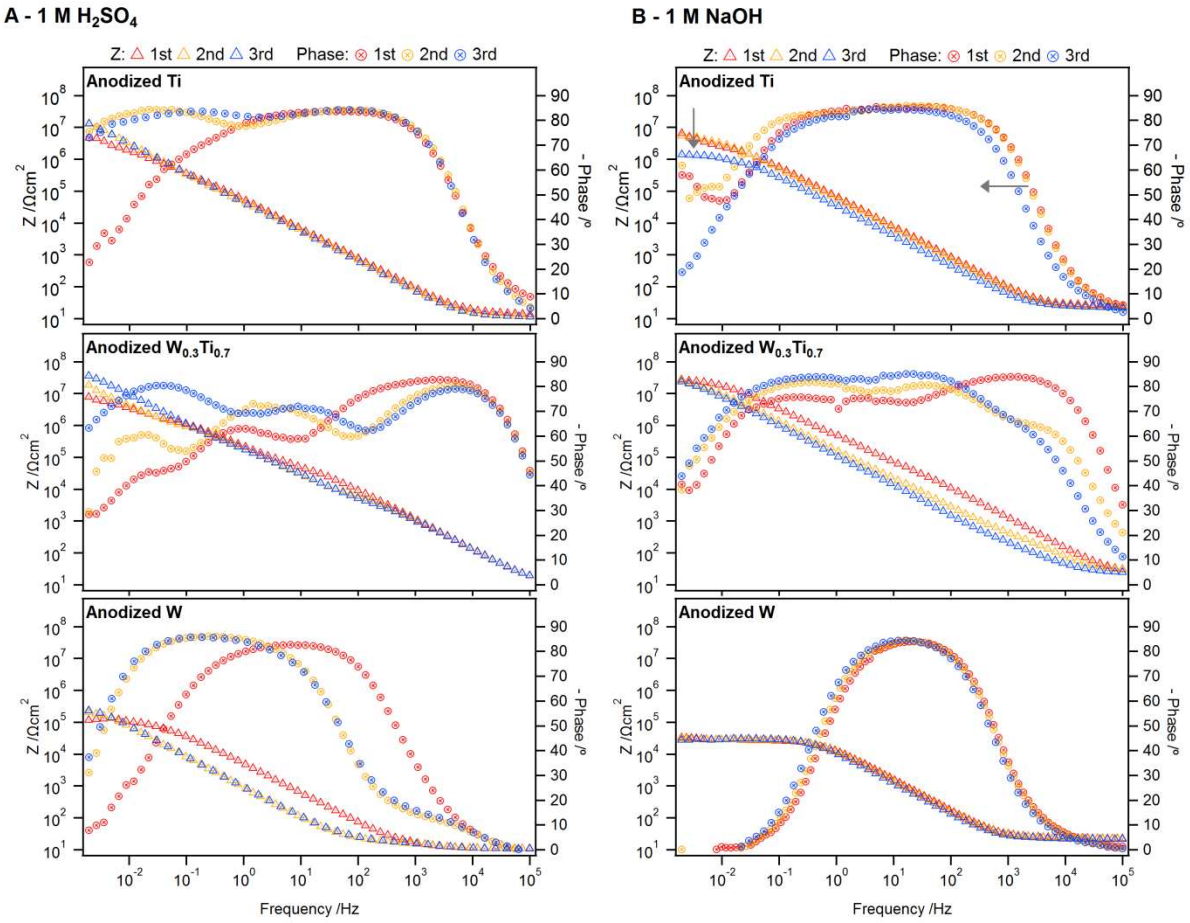

Figure 5: Bode plot representation of EIS on anodic oxides grown on different precursors. 3 consecutive EIS measurements were performed at OCP with 10 mV applied perturbation voltage over a total period of 6 h: **A)** Measurements in acidic solution (1 M H_2SO_4), **B)** Measurements in alkaline solution (1 M NaOH).

Figure 5 shows an EIS Bode plot representation of anodic oxides grown on pure Ti as well as $W_{0.3}Ti_{0.7}$ and W, in both acidic and alkaline solutions. The EIS measurements were performed at an interval of 2 h over a total period of 6 h. Differences in the spectra are due to reactions occurring on the oxide surface as a function of immersion time. In the case of dynamically changing systems which undergo a significant dissolution of the surface oxide a scientifically meaningful fitting of the EIS data using equivalent circuits is highly invested and beyond the scope of this work. For this reason we limit the analysis to a qualitative discussion of the most striking feature of the spectra. For anodized Ti a slight increase in impedance *Z* can be observed at low frequencies upon immersion in 1 M H_2SO_4, (**Figure 5A**). This can be explained by defects initially present in the anodic oxide, resulting in high leakage currents to the underlying metallic Ti layer. Between the first and second EIS measurement, this leakage current is reduced, whereas no changes are observed thereafter indicating the stabilization of the surface oxide. In

1 M NaOH, the TiO_2 layer appears to be less stable (**Figure 5B**). With each consecutive EIS measurement, the measured impedance at low frequencies is gradually dropping, accompanied by a phase shift at higher frequencies, which can be explained by a slow oxide dissolution with associated thinning of the oxide. The different stabilities of the anodic TiO_2 as function of pH have implications on the TiO_2 terminated oxides grown on alloy precursors. EIS of oxides grown on $W_{0.3}Ti_{0.7}$ precursors show a passive behavior in acidic environments whereas in alkaline solutions, a thinning of the protective TiO_2 surface layer is again observed. Oxides grown on pure W on the other hand are unstable in either media. While the WO_3 films are more stable in the acidic environment, which is in good agreement with literature reports of the WO_3 Pourbaix diagram,[4] the low impedance values at low frequencies and the continuous phase shift with each consecutive measurement indicate a slow dissolution of the material. These results highlight that the presence of a continuous surface TiO_2 layer is a necessary prerequiste for the chemical stability of the underlayaing mixed oxide.

The anodized alloy specimens were then subjected to potentiodynamic polarization in 1 M HCl or 1 M NaCl + 1 M NaOH for acidic and alkaline conditions, respectively (see **Figure 6**). These more aggressive electrolytes were chosen to provoke oxide breakdown upon polarization. More striking differences between the sample's corrosion behaviors can be observed upon polarization away from OCP. As expected, pure TiO_2 exhibits a passive behaviour. However, the current densities in both acidic and alkaline environments drastically increase with decreasing Ti content in the alloy precursor (note the exponential scale of the Y-axis in Fig. 6).

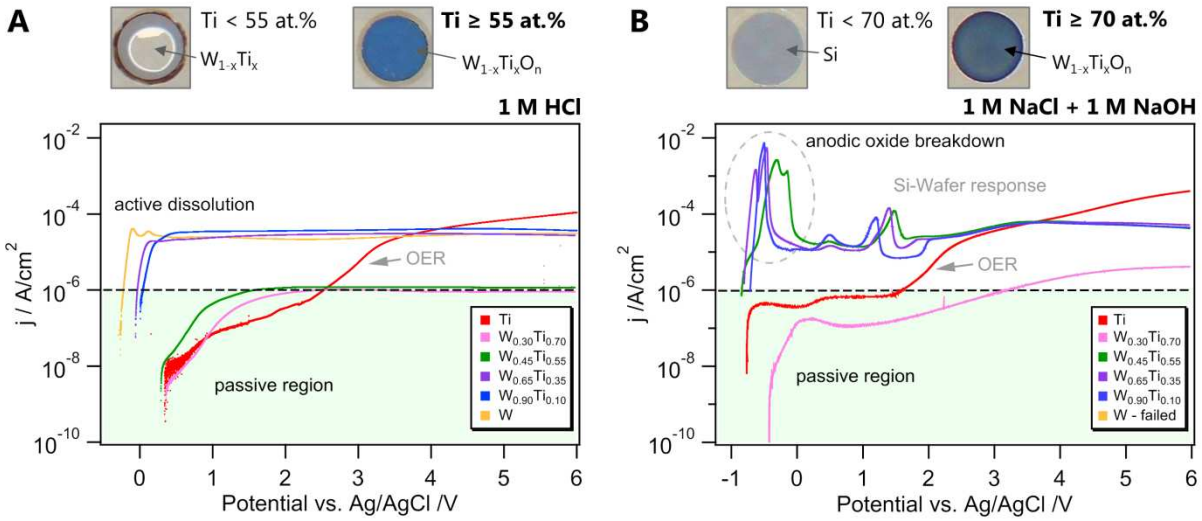

Figure 6: Potentiodynamic polarization measurements of anodic oxides grown on precursors of different alloying concentration (1 mV/s scan rate). A) in 1 M HCl: above 50at.% Ti, a dense protective surface layer stabilizes the film in acidic media B) in 1 M NaCl + 1 M NaOH: a thicker surface coating is necessary to sufficiently stabilize the anodic oxide. Oxides grown on pure W dissolved already during the EIS characterization period. Anodic oxides with low Ti concentrations actively dissolved and failed at relatively low polarization potentials. (The shaded area highlights current densities <1 µA/cm^2 indicating passive behavior). The pictures show representative samples after the measurements.

While samples with low Ti concentrations are dissolving even at low polarization voltages, a precursor composition of over 50% Ti appears to be sufficient to passivate the anodic oxides in the acidic environment. This observation is in excellent agreement with the respective threshold concentration of 50 at.% required to form a continuous TiO_2 film on the anodized oxide surface (**Figure 3**). In alkaline conditions, the Ti threshold concentration for achieving surface passivation appears to be higher than in acidic conditions: see **Figure 6B**. Pure WO_3 is already dissolved at the onset of the EIS measurement, so that no potentiodynamic polarization measurements could be conducted. For Ti alloy concentrations below 70 at.%, the potentiodynamic polarisation curves show anodic oxide breakdown and active dissolution at relatively low polarization potentials, followed by the typical footprint of Si dissolution (Si-substrates were used under the metallic precursors) at around 2.5 $V_{Ag/AgCl}$. Ti concentration as high as 70 at.%. (resulting in a considerably thicker passivating TiO_2 surface layer) are required to efficiently protect the underyling oxide phase from dissolution in alkaline solutions. This difference in anodized oxide stability behavior in the acidic and alkaline solutions is consistent with the known pH dependence of the stability of pure TiO_2.[37,38] The need for a thicker TiO_2 protective layer in alkaline media is also consistent with the observed degradation of the anodic TiO_2 grown on pure Ti, as well as the thinning of the TiO_2 surface layer on top of the oxide alloy in the case of $W_{0.3}Ti_{0.7}$ precursors (**Figure 5**). It is noted that for pure TiO_2, an increase in current

density is observed at polarization potentials above 2.5 V_{AgAgCl}. This current can be attributed to oxygen evolution reaction of the electrolyte (OER). Absence of this additional current density increase in the W-containing oxide bi-layers can be explained by a poor band alignment and the resulting interface recombination in the bilayer $W_{1-x}Ti_xO_n/TiO_2$ structure of the alloyed specimens.

4. Discussion and Conclusion

Anodizing of solid solution $W_{1-x}Ti_x$ alloy precursors in citric acid results in the formation of barrier-type (Ti,W)-oxide alloys, which are predominantly amorphous by XRD and TEM. The anodic oxides exhibit a varying degree of Ti-enrichment on the surface depending on both precursor composition and anodizing voltage. Anodizing of alloy precursors with Ti concentrations in excess of 50 at.% leads to the formation of a thin, but continuous TiO_2 surface layer as evidenced by XPS and (S)TEM analyses; the region underneath this TiO_2 film consists of a predominantly amorphous, homogeneous (W,Ti)-oxide alloy, with little compositional fluctuation. The thickness of the TiO_2 layer can be controlled via the anodizing voltage, whereas the composition of the underlying mixed oxide layer depends mostly on the precursor composition, which suggests that an independent control of the materials properties as well as the stability should be possible in this material system.

While the exact origin of the Ti surface enrichment has yet to be pinpointed, several possible mechanisms can be considered. One possible reason is the lower enthalpy of formation of TiO_2 ($\Delta_fH^{\ominus}(TiO_2\text{-rutile}) = -944$ kJ/mol) versus WO_3 ($\Delta_fH^{\ominus}(WO_3) = -843$ kJ/mol) as well as several other considered mixed oxide phases,[39] which could lead to a preferential formation of TiO_2 at the precursor-electrolyte interface. Another potentially contributing mechanism is the difference in diffusion coefficients for W and Ti. According to literature, the diffusion coefficient of W is significantly lower than that of Ti in both BCC Ti and BCC W.[40] Consequently, different concentration gradients of the respective ionic species could be established across the developing oxide layer during the early stages of anodizing (with oxide growth rates > 5 nm/s). This mechanism is also suggested by Habazaki *et al.* who observed a similar Ti surface enrichment, followed by a Ti-depletion region, in porous anodic oxides grown on $W_{0.20}Ti_{0.80}$ precursors.[31]

The different anodic oxide microstructures obtained as function of the anodizing voltage and the alloy precursor composition exhibit strikingly different stabilities in acidic and alkaline environments (**Figure 5**). As expected, both EIS and potentiodynamic polarization curves indicate a high stability and passive behavior of pure TiO_2 layers in acidic environments, whereas in alkaline media a degradation of pure TiO_2 occurs (see **Figure 6B**). In contrast, pure WO_3 is highly unstable in both of these environments. The stability of the $W_{1-x}Ti_xO_n$ oxide alloy correlates directly with the presence or absence of a TiO_2 surface film. The $W_{1-x}Ti_xO_n$ layers with a continuous TiO_2 film on their surface (for Ti alloy concentrations > 50 at.%) exhibit stable passive behavior in acidic media; whereas a thicker protective TiO_2 layer (as formed at even higher Ti alloy contents or anodizing potentials) is required in alkaline media.

Overall, the results of this work provide new insights into the anodizing behavior of $W_{1-x}Ti_x$ solid-solution alloys, with various applications in diverse fields from renewable energy generation to biomedical applications. More importantly, it is shown how controlled anodizing of self-passivating solid-solution alloy precursors can be utilized to produce oxide alloys with intrinsic protective surface films. The anodizing voltage can be varied to adjust the thickness of the passive surface-oxide layer, while the alloy precursor composition can be adjusted to control the underlying oxides chemical composition and phase constitution. These results suggest that an independent control of the functional properties and the stability of oxide alloys is possible by controlled oxidation of alloy precursors - a general design strategy that should be applicable to many other material systems.

Acknowledgements

The authors would like to thank Mirco Chiodi for support in the sample preparation and helpful discussions, Erwin Hack for the help with ellipsometry measurements as well as Vicente Araullo-Peters and Huan Ma for support with TEM specimen preparation. Funding from COST project IZCNZ0-174856 C16.0075, in the COST Action MP1407 (e-MINDS), the University of Zurich, the University Research Priority Program (URPP) LightChEC, and the Swiss National Science Foundation (AP Energy Grant # PYAPP2 160586) is gratefully acknowledged.

Supporting Information

Additional measurements and experimental details; Structural characterization: Stress

measurement on thin film precursors, (S)TEM analysis of the precursor, XRD-analysis of anodized films on fused silica, AFM-characterization of an anodized $W_{0.3}Ti_{0.7}$ alloy; Compositional analysis: Rutherford backscattering spectroscopy of anodized films, Detailed XPS investigation of anodic oxides grown on W and Ti, Surface-composition as a function of holding time during the anodizing process, XPS sputter depth profile of an anodized $W_{0.3}Ti_{0.7}$ alloy; Experimental details: Flow chart for the electrochemical assessment procedure.

References

(1) Fu, Q.; Tang, X.; Huang, B.; Hu, T.; Tan, L.; Chen, L.; Chen, Y. Recent Progress on the Long-Term Stability of Perovskite Solar Cells. *Advanced Science* **2018**, *5* (5), 1700387.

(2) Schneider, J.; Matsuoka, M.; Takeuchi, M.; Zhang, J.; Horiuchi, Y.; Anpo, M.; Bahnemann, D. W. Understanding TiO2 Photocatalysis : Mechanisms and Materials. *Chem. Rev.* **2014**, *114*, 9919–9986.

(3) Zheng, H.; Ou, J. Z.; Strano, M. S.; Kaner, R. B.; Mitchell, A.; Kalantar-Zadeh, K. Nanostructured Tungsten Oxide - Properties, Synthesis, and Applications. *Advanced Functional Materials* **2011**, *21* (12), 2175–2196.

(4) Lillard, R. S. The Nature of Oxide Films on Tungsten in Acidic and Alkaline Solutions. *Journal of The Electrochemical Society* **1998**, *145* (8), 2718.

(5) Sallard, S.; Brezesinski, T.; Smarsly, B. M. Electrochromic Stability of WO 3 Thin Films with Nanometer-Scale Periodicity and Varying Degrees of Crystallinity. *The Journal of Physical Chemistry C* **2007**, *111* (19), 7200–7206.

(6) Zhao, J.; Olide, E.; Osterloh, F. E. Enhancing Majority Carrier Transport in WO3 Water Oxidation Photoanode via Electrochemical Doping. *Journal of the Electrochemical Society* **2014**, *162* (1), H65–H71.

(7) Meléndez-Ceballos, A.; Fernández-Valverde, S. M.; Barrera-Díaz, C.; Albin, V.; Lair, V.; Ringuedé, A.; Cassir, M. TiO2 Protective Coating Processed by Atomic Layer Deposition for the Improvement of MCFC Cathode. *International Journal of Hydrogen Energy* **2013**, *38* (30), 13443–13452.

(8) Moehl, T.; Suh, J.; Sévery, L.; Wick-Joliat, R.; Tilley, S. D. Investigation of (Leaky) ALD TiO2 Protection Layers for Water-Splitting Photoelectrodes. *ACS Applied Materials & Interfaces* **2017**, *9* (50), 43614–43622.

(9) Yu, Y.; Sun, C.; Yin, X.; Li, J.; Cao, S.; Zhang, C.; Voyles, P. M.; Wang, X. Metastable Intermediates in Amorphous Titanium Oxide: A Hidden Role Leading to Ultra-Stable Photoanode Protection. *Nano Letters* **2018**, *18* (8), 5335–5342.

(10) Siol, S.; Holder, A.; Steffes, J.; Schelhas, L. T.; Stone, K. H.; Garten, L.; Perkins, J. D.; Parilla, P. A.; Toney, M. F.; Huey, B. D.; Tumas, W.; Lany, S.; Zakutayev, A. Negative-Pressure Polymorphs Made by Heterostructural Alloying. *Science Advances* **2018**, *4* (4), eaaq1442.

(11) Wen, R.-T.; Granqvist, C. G.; Niklasson, G. A. Eliminating Degradation and Uncovering Ion-Trapping Dynamics in Electrochromic WO3 Thin Films. *Nature Materials* **2015**, *14* (10), 996–1001.

(12) Arvizu, M. A.; Triana, C. A.; Stefanov, B. I.; Granqvist, C. G.; Niklasson, G. A.

Electrochromism in Sputter-Deposited W-Ti Oxide Films: Durability Enhancement due to Ti. *Solar Energy Materials and Solar Cells* **2014**, *125* (2508), 184–189.

(13) Siol, S. Accessing Metastability in Heterostructural Semiconductor Alloys. *Phys. Status Solidi A* **2019**, 1800858.

(14) Siol, S.; Holder, A.; Ortiz, B. R.; Parilla, P. A.; Toberer, E.; Lany, S.; Zakutayev, A. Solubility Limits in Quaternary SnTe-Based Alloys. *RSC Advances* **2017**, *7* (40), 24747–24753.

(15) Foley, R. T. Localized Corrosion of Aluminum Alloys—A Review. *CORROSION* **1986**, *42* (5), 277–288.

(16) Beni, A.; Ott, N.; Ura-Bińczyk, E.; Rasinski, M.; Bauer, B.; Gille, P.; Ulrich, A.; Schmutz, P. Passivation and Localised Corrosion Susceptibility of New Al–Cr–Fe Complex Metallic Alloys in Acidic NaCl Electrolytes. *Electrochimica Acta* **2011**, *56* (28), 10524–10532.

(17) Cancellieri, C.; Evangelisti, F.; Geldmacher, T.; Araullo-Peters, V.; Ott, N.; Chiodi, M.; Döbeli, M.; Schmutz, P. The Role of Si Incorporation on the Anodic Growth of Barrier-Type Al Oxide. *Materials Science and Engineering: B* **2017**, *226* (June), 120–131.

(18) Habazaki, H.; Skeldon, P.; Shimizu, K.; Thompson, G. E.; Wood, G. C. Anodic Film Formation on Sputter-Deposited Amorphous Al-Zr Alloys. *Journal of Physics D: Applied Physics* **1995**, *28* (12), 2612–2618.

(19) Wegener, T.; Klein, F.; Litnovsky, A.; Rasinski, M.; Brinkmann, J.; Koch, F.; Linsmeier, C. Development and Analyses of Self-Passivating Tungsten Alloys for DEMO Accidental Conditions. *Fusion Engineering and Design* **2017**, *124*, 183–186.

(20) Koch, F.; Bolt, H. Self Passivating W-Based Alloys as Plasma Facing Material for Nuclear Fusion. *Physica Scripta* **2007**, *T128*, 100–105.

(21) Hu, S.; Shaner, M. R.; Beardslee, J. A.; Lichterman, M.; Brunschwig, B. S.; Lewis, N. S. Amorphous TiO2 Coatings Stabilize Si, GaAs, and GaP Photoanodes for Efficient Water Oxidation. *Science* **2014**, *344* (6187), 1005–1009.

(22) de Tacconi, N. R.; Chenthamarakshan, C. R.; Yogeeswaran, G.; Watcharenwong, A.; De Zoysa, R. S.; Basit, N. A.; Rajeshwar, K. Nanoporous TiO2 and WO3 Films by Anodization of Titanium and Tungsten Substrates: Influence of Process Variables on Morphology and Photoelectrochemical Response. *The Journal of Physical Chemistry B* **2006**, *110* (50), 25347–25355.

(23) Bendova, M.; Gispert-Guirado, F.; Hassel, A. W.; Llobet, E.; Mozalev, A. Solar Water Splitting on Porous-Alumina-Assisted TiO2-Doped WOx Nanorod Photoanodes: Paradoxes and Challenges. *Nano Energy* **2017**, *33* (November 2016), 72–87.

(24) Reyes-Gil, K. R.; Stephens, Z. D.; Stavila, V.; Robinson, D. B. Composite WO3/TiO2 Nanostructures for High Electrochromic Activity. *ACS Applied Materials and Interfaces* **2015**, *7* (4), 2202–2213.

(25) Nah, Y. C.; Shrestha, N. K.; Kim, D.; Schmuki, P. Electrochemical Growth of Self-Organized TiO2-WO3 Composite Nanotube Layers: Effects of Applied Voltage and Time. *Journal of Applied Electrochemistry* **2013**, *43* (1), 9–13.

(26) Regonini, D.; Bowen, C. R.; Jaroenworaluck, A.; Stevens, R. A Review of Growth Mechanism, Structure and Crystallinity of Anodized TiO2 Nanotubes. *Materials Science and Engineering R: Reports* **2013**, *74* (12), 377–406.

(27) Chiu, Y.-H.; Lai, T.-H.; Chen, C.-Y.; Hsieh, P.-Y.; Ozasa, K.; Niinomi, M.; Okada, K.; Chang, T.-F. M.; Matsushita, N.; Sone, M.; Hsu, Y.-J. Fully Depleted Ti–Nb–Ta–Zr–O Nanotubes: Interfacial Charge Dynamics and Solar Hydrogen Production. *ACS Applied Materials & Interfaces* **2018**, *10* (27), 22997–23008.

(28) Allam, N. K.; Alamgir, F.; El-Sayed, M. A. Enhanced Photoassisted Water Electrolysis Using Vertically Oriented Anodically Fabricated Ti−Nb−Zr−O Mixed Oxide Nanotube Arrays. *ACS Nano* **2010**, *4* (10), 5819–5826.

(29) Habazaki, H.; Skeldon, P.; Shimizu, K.; Thompson, G. E.; Wood, G. C. Anodic Film Formation on a Sputter-Deposited Al-30at%Mo Alloy. *Corrosion Science* **1995**, *37* (9), 1497–1509.

(30) Nah, Y.-C.; Ghicov, A.; Kim, D.; Berger, S.; Schmuki, P. TiO2 −WO3 Composite Nanotubes by Alloy Anodization: Growth and Enhanced Electrochromic Properties. *Journal of the American Chemical Society* **2008**, *130* (48), 16154–16155.

(31) Lu, Q.; Alberch, J.; Hashimoto, T.; Garcia-Vergara, S. J.; Habazaki, H.; Skeldon, P.; Thompson, G. E. Porous Anodic Oxides on Titanium and on a Ti–W Alloy. *Corrosion Science* **2008**, *50* (2), 548–553.

(32) Evangelisti, F.; Stiefel, M.; Guseva, O.; Partovi Nia, R.; Hauert, R.; Hack, E.; Jeurgens, L. P. H.; Ambrosio, F.; Pasquarello, A.; Schmutz, P.; Cancellieri, C. Electronic and Structural Characterization of Barrier-Type Amorphous Aluminium Oxide. *Electrochimica Acta* **2017**, *224*, 503–516.

(33) Vegard, L. Die Konstitution Der Mischkristalle Und Die Raumfüllung Der Atome. *Zeitschrift für Physik* **1921**, *5* (1), 17–26.

(34) Jin, Z.; Qiu, C. Thermodynamic Evaluation of Ti–W System. *Materials Science and Technology* **1993**, *9* (5), 378–383.

(35) Gonzalez-Castano, M.; Döbeli, M.; Araullo-peters, V.; Jeurgens, L. P. H.; Schmutz, P.; Cancellieri, C. Substrate Purity Effect on the Defect Formation and Properties of Amorphous Anodic Barrier Al2O3. **2018**, *165* (7), 422–432.

(36) Jain, A.; Ong, S. P.; Hautier, G.; Chen, W.; Richards, W. D.; Dacek, S.; Cholia, S.; Gunter, D.; Skinner, D.; Ceder, G.; Persson, K. A. Commentary: The Materials Project: A Materials Genome Approach to Accelerating Materials Innovation. *APL Materials* **2013**, *1* (1), 11002.

(37) Chen, C.-C.; Chen, J.-H.; Chao, C.-G.; Say, W. C. Electrochemical Characteristics of Surface of Titanium Formed by Electrolytic Polishing and Anodizing. **2005**, *40*, 4053–4059.

(38) Mills, A.; Worsley, D.; Davies, R. H. Effect of pH on the Stability of TiO2 Coatings on Glass Photocatalysis Reactors for Water Purification. *Journal of the Chemical Society, Chemical Communications* **1994**, *0* (23), 2677.

(39) Thermodynamic Properties of Compounds. In *Landolt-Börnstein - Group IV Physical Chemistry*; Springer-Verlag: Berlin/Heidelberg, 2001.

(40) Neumann, G.; Tuijn, C. *Self-Diffusion and Impurity Diffusion in Pure Metals: Handbook of Experimental Data*, 14th ed.; Elsevier, 2008.

TOC-Figure:

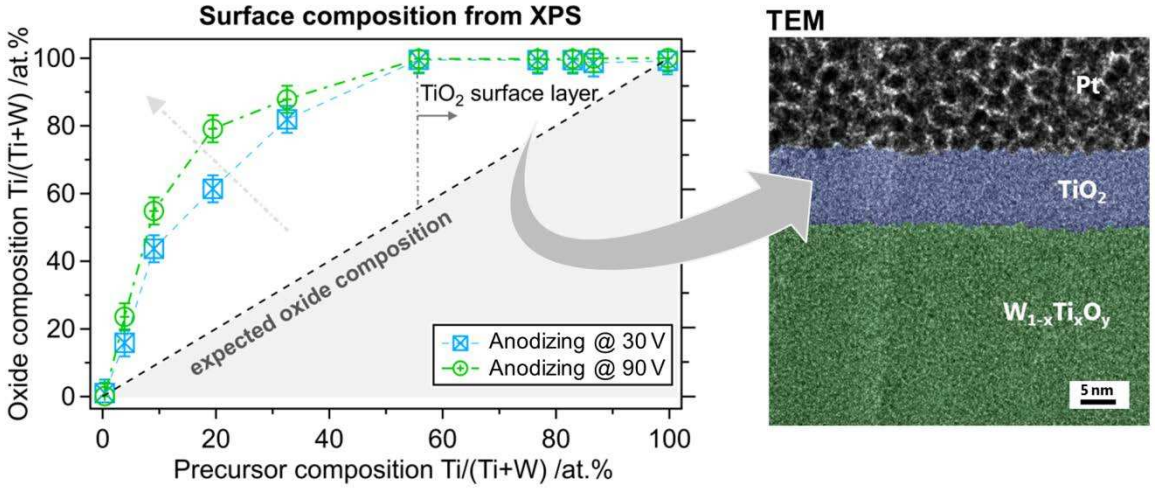
Surface composition from XPS
Oxide composition Ti/(Ti+W) /at.%
Precursor composition Ti/(Ti+W) /at.%
0
20
40
60
80
100
TiO2 surface layer
expected oxide composition
Anodizing @ 30 V
Anodizing @ 90 V
TEM
Pt
TiO2
W1-xTixOy
5 nm